Journal of Liquid Chromatography & Related Technologies

ISSN: 1082-6076 (Print) 1520-572X (Online) Journal homepage: https://www.tandfonline.com/loi/ljlc20

# Linearized non-equilibrium and non-isothermal two-dimensional model of liquid chromatography for studying thermal effects in cylindrical columns

Abdulaziz Garba Ahmad, Shamsul Qamar & Andreas Seidel-Morgenstern

**To cite this article:** Abdulaziz Garba Ahmad, Shamsul Qamar & Andreas Seidel-Morgenstern (2019) Linearized non-equilibrium and non-isothermal two-dimensional model of liquid chromatography for studying thermal effects in cylindrical columns, Journal of Liquid Chromatography & Related Technologies, 42:13-14, 436-451, DOI: 10.1080/10826076.2019.1625370

**To link to this article:** https://doi.org/10.1080/10826076.2019.1625370

Published online: 18 Jun 2019.

JOURNAL OF LIQUID CHROMATOGRAPHY & RELATED TECHNOLOGIES
2019, VOL. 42, NOS. 13–14, 436–451
https://doi.org/10.1080/10826076.2019.1625370

Taylor & Francis
Taylor & Francis Group



# Linearized non-equilibrium and non-isothermal two-dimensional model of liquid chromatography for studying thermal effects in cylindrical columns

Abdulaziz Garba Ahmad[a,b], Shamsul Qamar[a,c], and Andreas Seidel-Morgenstern[c]

[a]Department of Mathematics, COMSATS University Islamabad, Islamabad, Pakistan; [b]Department of Mathematics Programme, National Mathematical Centre Abuja, Abuja, Nigeria; [c]Max Planck Institute for Dynamics of Complex Technical Systems, Magdeburg, Germany

**ABSTRACT**

A non-equilibrium and non-isothermal two-dimensional lumped kinetic model (2 D-LKM) is formulated and analytically solved to study the influence of temperature variations along the axial and radial coordinates of a liquid chromatographic column. The model includes convection-diffusion partial differential equations for mass and energy balances in the mobile phase coupled with differential equations for mass and energy in the stationary phase. The solutions are derived analytically through sequential implementation of finite Hankel and Laplace transformations using the Dirichlet inlet boundary conditions. The coupling between the thermal waves and concentration fronts is demonstrated through numerical simulations and important parameters are recognized that influence the column performance. For a more comprehensive study of the considered model, numerical temporal moments are obtained from the derived solutions. Several case studies are conducted and validity ranges of the derived analytical solutions are identified. The current analytical results will play a major role in the improvements of non-equilibrium and non-isothermal liquid chromatographic processes.

**KEYWORDS**

Affinity; analytical solutions; axial and radial dispersions; non-isothermal chromatography; two-dimensional lumped kinetic model

**GRAPHICAL ABSTRACT**

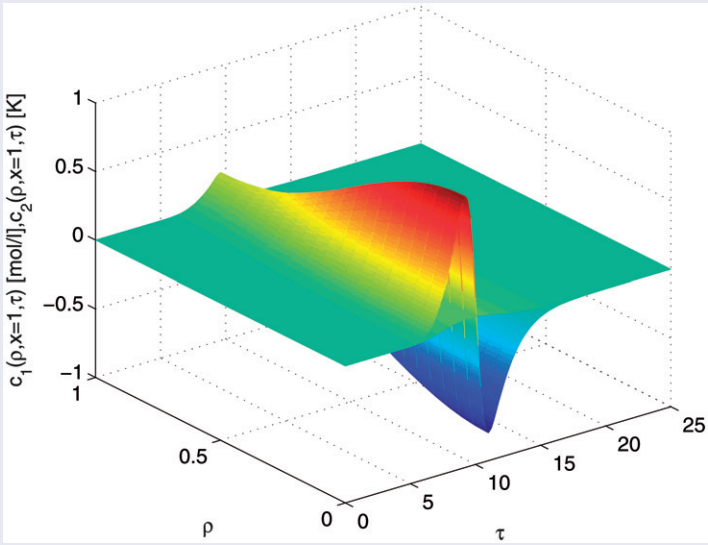


## Introduction

Column chromatography technique is a useful tool for the separation of multi-component mixtures in which the adsorption affinities of the components are dissimilar. This technique is frequently utilized in the pharmaceutical, food and chemical industries where the conventional thermal unit operations, such as extraction and distillation, are not suitable [1–5]. This process is equally popular at large and preparative scales, especially for purifying proteins and other high-value products.

All chromatographic techniques are broadly affected by temperature and there are several ways to reveal its importance. For instance, elevated temperature reduces viscosity and enhances solubility and diffusivity [6,7]. Temperature

CONTACT Shamsul Qamar shamsul.qamar@comsats.edu.pk Department of Mathematics, COMSATS University Islamabad, Islamabad, Pakistan.
Color versions of one or more of the figures in the article can be found online at www.tandfonline.com/ljlc.

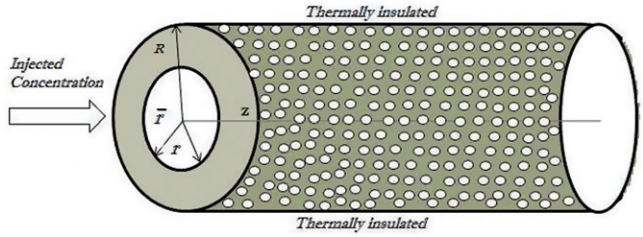


**Figure 1.** Diagram of the thermally insulated column considering the solute injection either through the inner cylindrical core or through the outer annular ring.

**Table 1.** Values of the model parameters used in the test problems

| Parameters | Values |
|---|---|
| Interstitial velocity | $u = 1.5$ cm/min |
| Column length | $L = 4.0$ cm |
| Porosity | $\epsilon = 0.4$ |
| Density of heat capacity of solid | $c_f = 4$ kJ/l |
| Density of heat capacity of liquid | $c_e = 4$ kJ/l |
| Axial dispersion coefficient | $D_z = 0.025$ cm$^2$/min |
| Axial conductivity coefficient | $\lambda_z = 0.1$ kJcm$^{-1}$min$^{-1}$ |
| Radial dispersion coefficient | $D_r = 0.0025$ cm$^2$/min |
| Radial conductivity coefficient | $\lambda_r = 0.01$ kJcm$^{-1}$min$^{-1}$ |
| Mass transfer coefficient | $k = 1$ cm/min |
| Heat transfer coefficient | $h_p = 1$ $W$(cm$^2$K)$^{-1}$ |
| Initial temperature | $T_{\text{init}} = 300$ K |
| Initial concentration | $c_{\text{init}} = 0$ mol/l |
| Inlet concentration | $c_{\text{inj}} = 1$ mol/l |
| Reference temperature | $T_{\text{ref}} = 300$ K |
| Inlet temperature | $T_{\text{inj}} = 300$ K |
| Adsorption equilibrium constant | $a_{ref} = 1$ |
| Dimensionless injection time | $\tau_{\text{inj}} = 1$ min |

influences column efficiency, retention time, peak shape, and total time analysis, because thermodynamics and adsorption kinetics are depending on the temperature. Further, operation of the process under a controlled temperature improves reproducibility. Although, thermal effects are usually neglected in the liquid chromatographic columns by assuming the influence of adsorption heat insignificant, more and more chromatographers have started realizing the temperature as imperative to the optimization of the process [8–10]. On the other hand, several authors have studied thermal effects in the gas chromatography [11–14]. Further contributions on the study of thermal effects in liquid chromatographic columns are also available in the literature [5,9,10,15–23].

Several kinds of mathematical models exist in the literature for simulating liquid chromatography process considering different levels of complexities. Out of them, the important and frequently used models contain the equilibrium dispersive model (EDM), the linear driving force model, the lumped kinetic model (LKM) and the general rate model (GRM) [1,4–6,24–26]. The mass transfer rate is assumed infinite in the EDM, while the rate of change of local concentration is considered finite in the LKM [1,4,5]. The GRM is regarded as the most comprehensive model which incorporates the interfacial mass transfer between the stationary and mobile phases, as well as the intra particle diffusion [1].

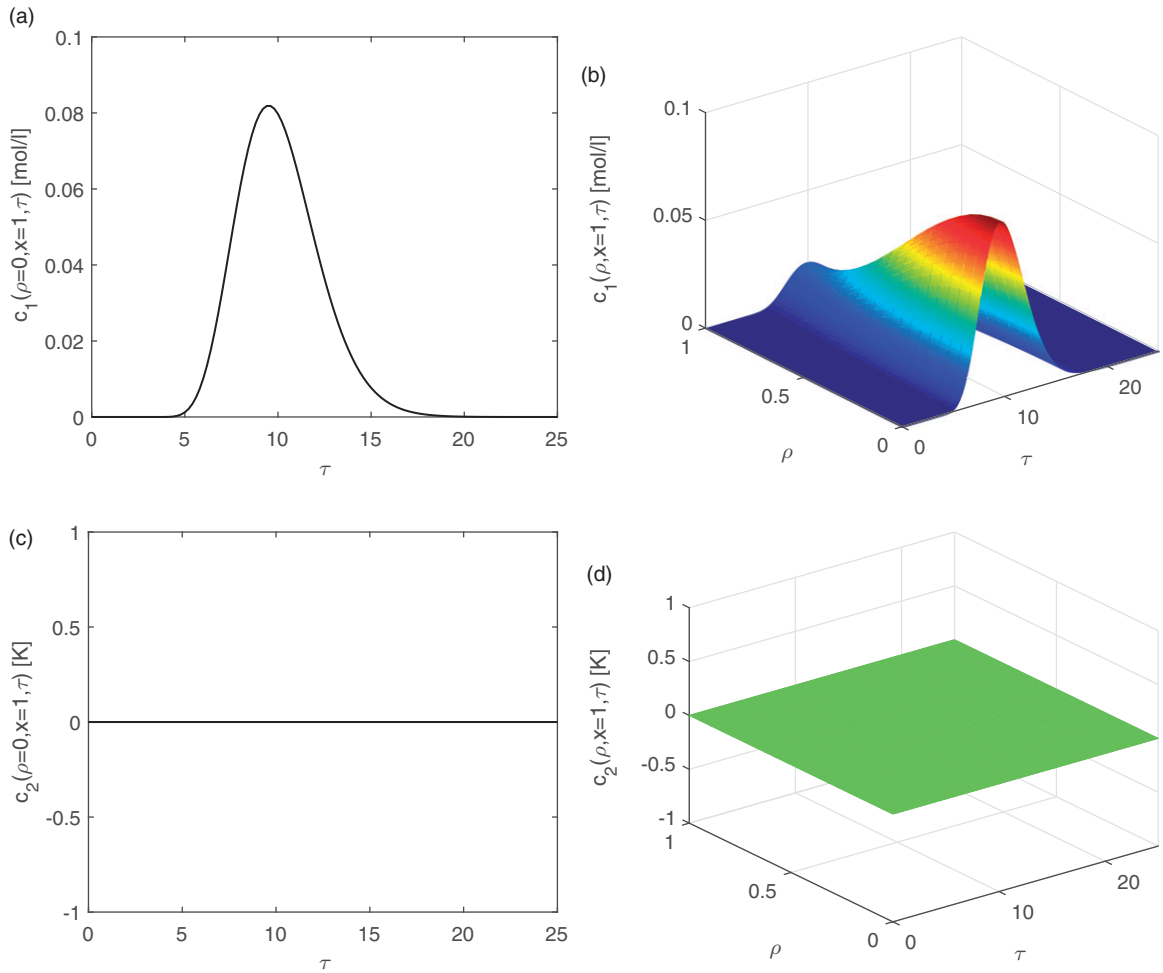


**Figure 2.** Plots of profiles for the Isothermal case $(\Delta H_A = 0\ kJ/mol)$. Inner zone injection and parameters of the Table 1 are considered.

The linear models are solvable analytically and several authors have derived the analytical solutions of linear one-dimensional (1 D) models [27–35]. Moreover, the analytical solutions of linearized isothermal two-dimensional (2 D) models are also available in the literature [36–39]. It was found that the developed 2 D-models and their solutions are more flexible and general than the classical 1 D-models and their solutions. The solutions of 2 D-models can be utilized for studying both axial and radial concentration gradients inside the columns. They are useful when the injection is imperfect at the column inlet or column is packed non-homogeneously. Moreover, experiment studies on the implementation of 2 D liquid chromatography are also available in the literature which further motivate the interest of analytical chemist in the current theoretical study [40,41].

In this article, a linearized non-isothermal 2 D-LKM is solved analytically. The present work further generalizes our preceding analysis for the non-isothermal 1 D-LKM [42]. Contrary to the previous analysis, the current flexible and general non-isothermal 2 D-LKM allows the study of both axial and radial concentration and temperature gradients inside the column. Such a non-isothermal model is very useful for quantifying radial temperature gradients in those columns in which radial concentration gradients are significant. The Hankel and Laplace transformations are jointly used to obtain the Hankel-Laplace domains analytical solutions [36–39]. An accurate and efficient procedure of numerical Laplace inversion is applied to obtain solutions in the time domain [43]. A few important case studies are conducted to demonstrate the joint occurrence of thermal and concentration fronts. Moreover, those key parameters are pointed out which influence the temperature gradients inside the column.

The organizations of the paper contents are as follows. In Section 2, a non-equilibrium and non-isothermal 2 D-LKM is formulated to simulate dynamical processes in non-isothermal liquid chromatographic columns of cylindrical geometry. In Section 3, the analytical solutions of the 2 D-model are derived for the considered Dirichlet boundary conditions. Section 4 presents some numerical test problems and eventually conclusions are given in Section 5.

## The non-isothermal 2 D-LKM chromatographic model

In the derivation of the model, it is assumed that i) the chromatographic column is thermally insulated and packed homogeneously with spherical particles of radius $R_p$ as

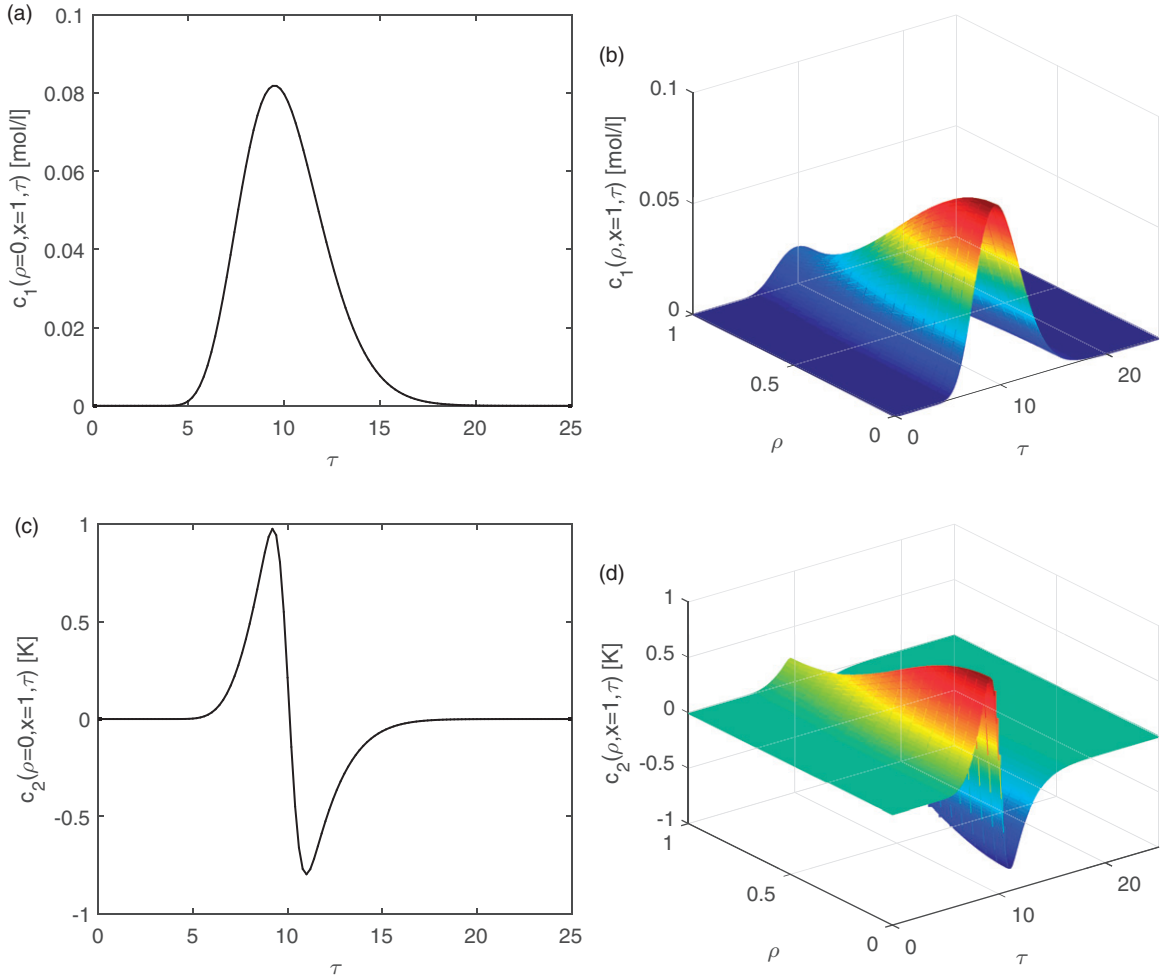


**Figure 3.** Plots of profiles for the non-Isothermal case ($\Delta H_A = -10\ kJ/mol$). Inner zone injection and parameters of the Table 1 are considered.

shown in Figure 1 [44,45], ii) the volumetric flow rate is constant, iii) the fluid is incompressible and interaction between the mobile and stationary phases are negligible, iv) the viscous heat of the system is neglected, v) the axial and radial heat conductivity coefficients are independent of the flow rate, vi) the temperature has no influence on the physical properties like density, viscosity, heat capacity and transport coefficients (e.g. axial and radial dispersions and heat conductivities), vii) the overall adsorption rate is expressed by the linear driving force model, and viii) the solid phase heat transfer resistance is concentrated at the particle surface.

Let the time coordinate is denoted by $t$, the radial coordinate across the column radius is represented by $r$, while the axial coordinate along the column length is symbolized as $z$. The solute propagates along $z$-direction of the column by advection and axial-dispersion, while radial-dispersion is only responsible for its spreading along the column radius. Two different modes of injection are considered for triggering radial gradients inside the column. A new symbol $\bar{r}$ is introduced for splitting the inlet cross-section of the column into outer annular and inner cylindrical regions. Thus, three different possibilities are available for sample injection into the column, i.e. the sample can be either injected via inner region, outer region, or via full cross-sectional area of the column. The latter possibility fulfills when the value of $\bar{r}$ is equal to the radius of the column represented by $R$. The mass and heat balance equations for a single-component elution in the mobile phase are stated as

$$\frac{\partial c}{\partial t}+u\frac{\partial c}{\partial z}=D_z\frac{\partial^2 c}{\partial z^2}+D_r\left(\frac{\partial^2 c}{\partial r^2}+\frac{1}{r}\frac{\partial c}{\partial r}\right)-Fk(q^*-q), \tag{1}$$

$$\frac{\partial T}{\partial t}+u\frac{\partial T}{\partial z}=\frac{\lambda_z}{c_f}\frac{\partial^2 T}{\partial z^2}+\frac{\lambda_r}{c_f}\left(\frac{\partial^2 T}{\partial r^2}+\frac{1}{r}\frac{\partial T}{\partial r}\right)$$

$$+F\frac{-\Delta H_A}{c_f}\frac{\partial q}{\partial t}-F\frac{c_e}{c_f}\frac{\partial T_s}{\partial t}. \tag{2}$$

In these equations, the solute concentration in the liquid phase is denoted by $c$, the interstitial velocity is represented as $u$, the axial-dispersion coefficient is denoted by $D_z$, the radial-dispersion coefficient is represented by $D_r$, while the phase ratio is defined as $F=\frac{1-\epsilon}{\epsilon}$ with $\epsilon$ being the external porosity. The symbol $k$ denotes the mass transfer rate coefficient, the non-equilibrium mean loading of solute in the solid phase is symbolized as $q$, a symbol $T$ is used for temperature of the mobile phase, the symbols $\lambda_z$ and $\lambda_r$ are

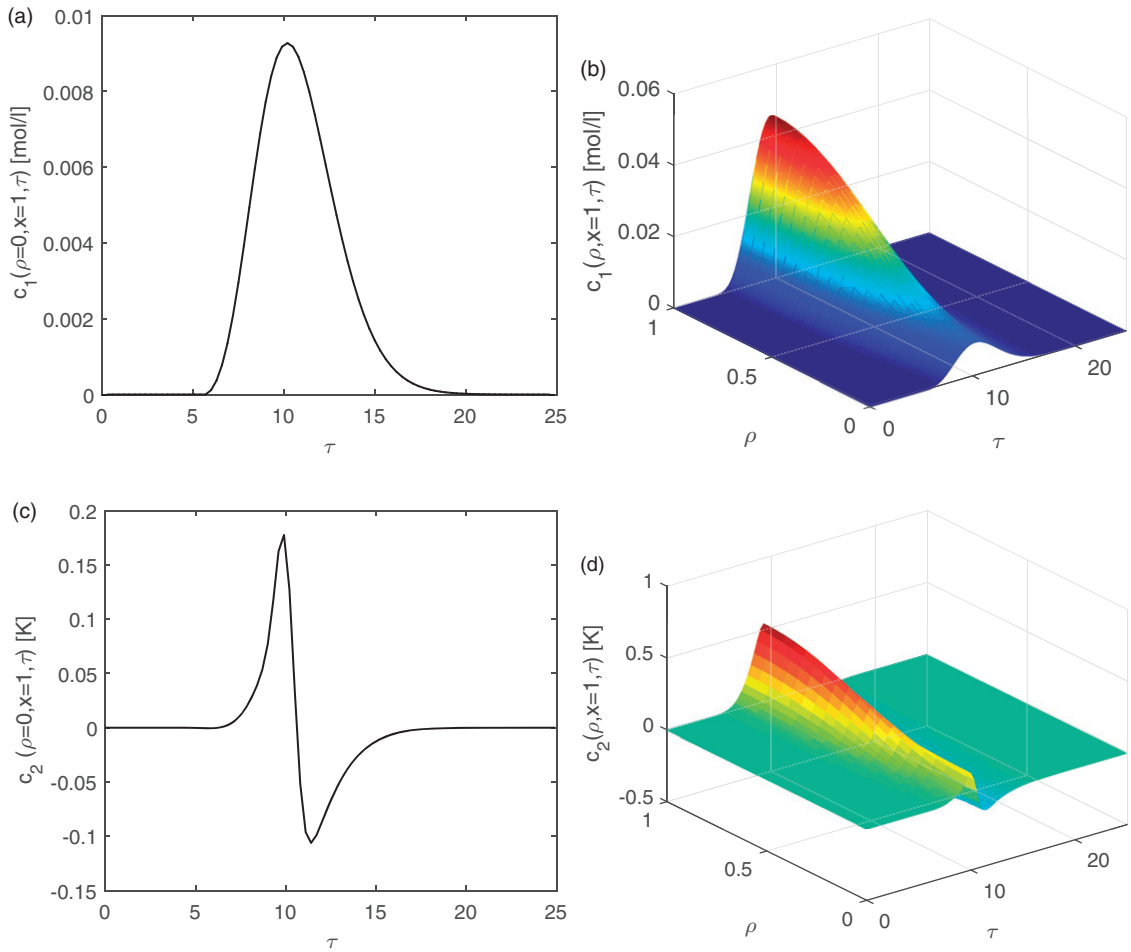


**Figure 4.** Plots of profiles for the non-isothermal case ($\Delta H_A=-10\ kJ/mol$). Outer zone injection and parameters of the Table 1 are considered.

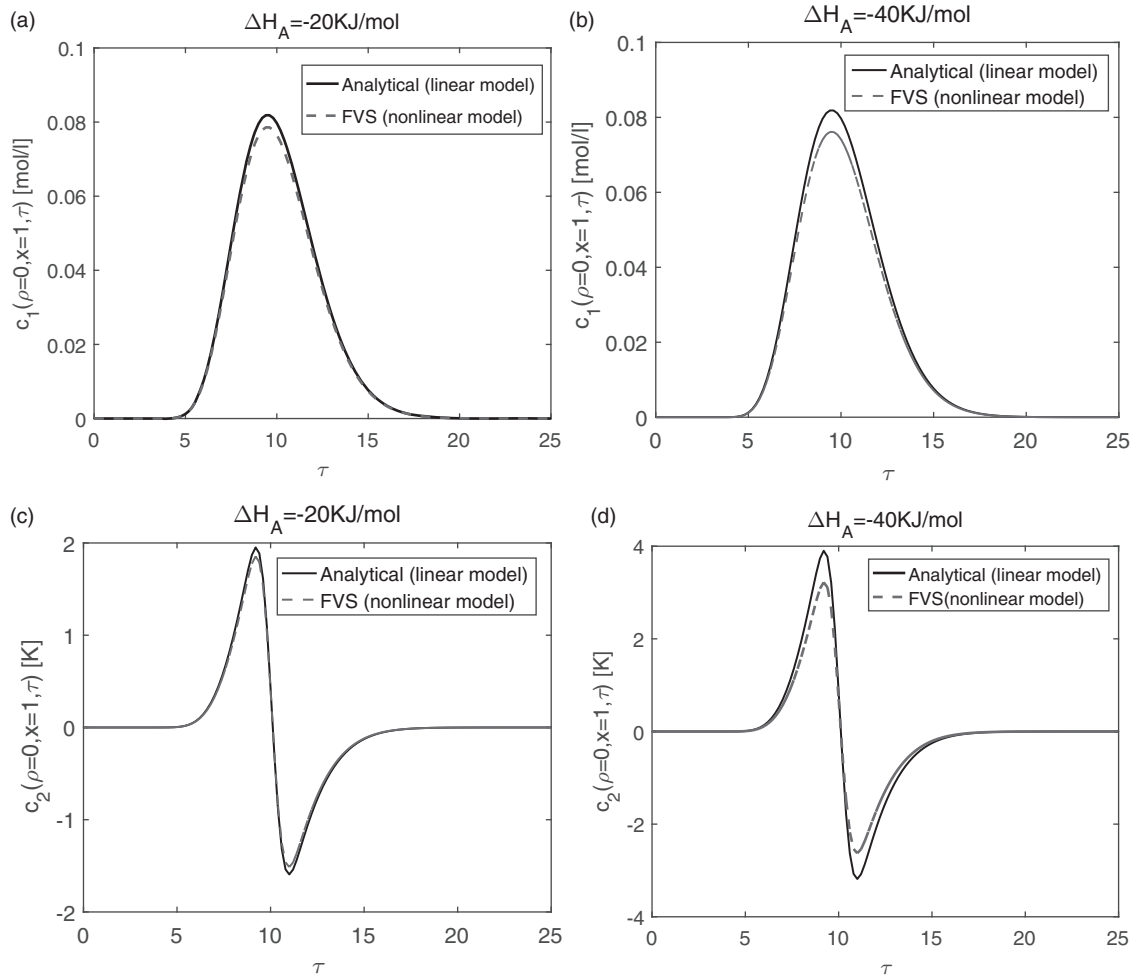


**Figure 5.** Comparison of analytical solutions for the linear isotherm and numerical solutions for the nonlinear isotherm at $\Delta H_A = -20\ kJ/mol$ and $\Delta H_A = -40\ kJ/mol$. Inner zone injection and parameters of the Table 1 are considered.

reserved for heat conductivity coefficients along the axial and radial coordinates. Furthermore, $c_e = \rho^s c_p^s$, $c_f = \rho^l c_p^l$, $\rho^s$ and $\rho^l$ respectively represent densities per unit volume in the solid and liquid phases, $c_p^s$ and $c_p^l$ respectively represent the corresponding heat capacities of the solid and liquid phases, while $T_s$ is utilized for temperature of the solid phase.

The corresponding mass and heat balance equations in the solid phase are expressed as

$$\frac{\partial q}{\partial t} = k(q^* - q), \tag{3}$$

$$\frac{\partial T_s}{\partial t} = \frac{-\Delta H_A}{c_e}\frac{\partial q}{\partial t} + \frac{3h_p}{R_p c_e}(T - T_S). \tag{4}$$

Here, $\Delta H_A$ symbolizes the enthalpy of adsorption and $h_p$ is used as a heat transfer coefficient between the mobile and solid phases. A temperature dependent relation between the solid phase equilibrium concentration $q^*$ and the liquid phase concentration $c$ is expressed as

$$q^* = a_{ref} \exp\left[\frac{-\Delta H_A}{R_g}\left(\frac{1}{T_s} - \frac{1}{T_{ref}}\right)\right] c. \tag{5}$$

Here, $T_{ref}$ represents the reference temperature, $a_{ref}$ is Henry's constant, and $R_g$ is a universal gas constant. To facilitate our analysis, the following new dependent variables are considered:

$$c_1 = c, \quad q_1 = q, \quad c_2 = T - T_{ref}, \quad q_2 = T_s - T_{ref}. \tag{6}$$

Furthermore, the following new dimensionless parameters are introduced in the model for minimizing the number of parameters:

$$\kappa = \frac{Lk}{u}, \quad \rho = \frac{r}{R}, \quad Pe_{z,H} = \frac{c_f L u}{\lambda_z}, \quad x = \frac{z}{L},$$

$$Pe_{\rho,H} = \frac{c_f R^2 u}{\lambda_r L}, \quad \tau = \frac{ut}{L}, \quad Pe_{z,M} = \frac{Lu}{D_z}, \quad Pe_{\rho,M} = \frac{R^2 u}{D_r L},$$

$$\beta_s = \frac{3Lh_p}{uR_p c_e}, \quad \beta_L = \frac{3Lh_p}{uR_p c_f}, \tag{7}$$

where the column length is denoted by $L$, the Peclet numbers of heat and mass transfer along the axial direction are respectively denoted by $Pe_{z,H}$ and $Pe_{z,M}$. While, $Pe_{\rho,H}$ and $Pe_{\rho,M}$ are the Peclet numbers of heat and mass transfer along the radial direction, respectively. On using Eqs. (6) and (7) in Eqs. (1)-(4), we obtain after some manipulations

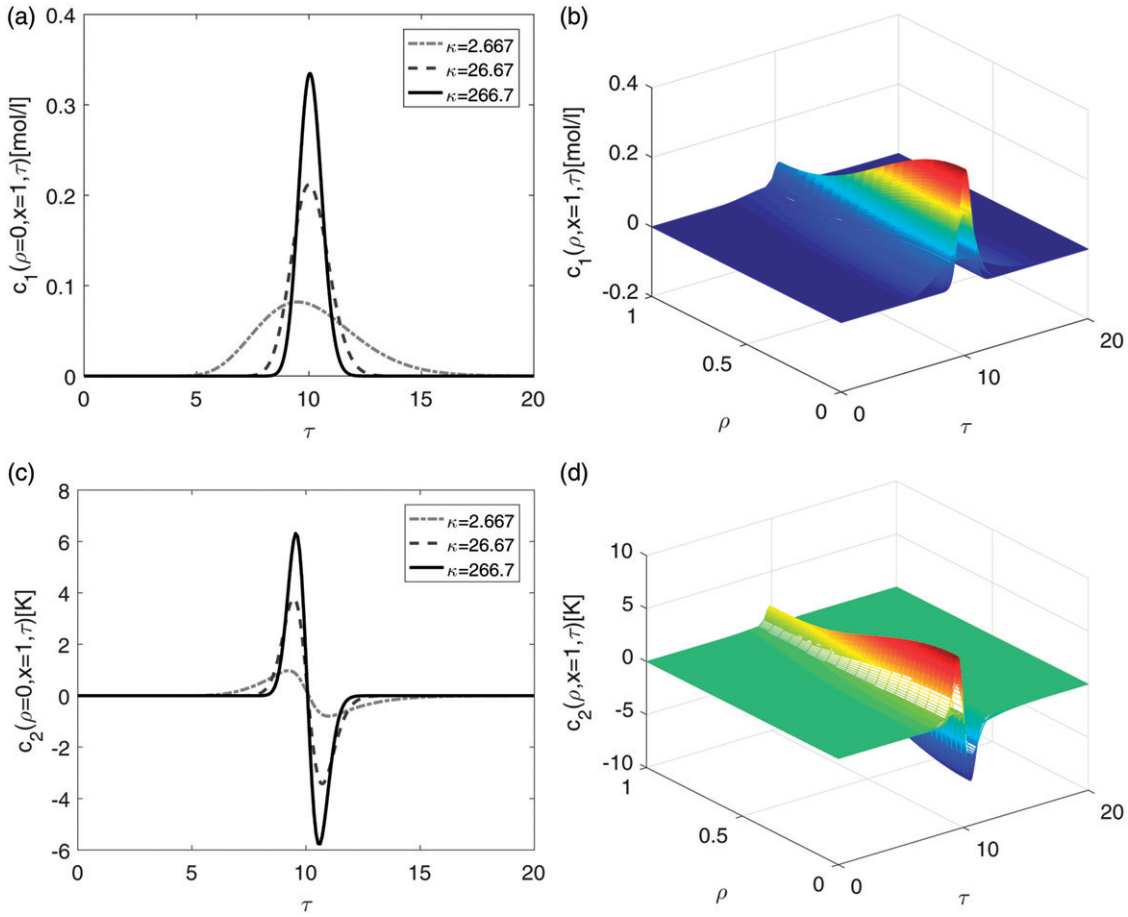


**Figure 6.** Effect of mass transfer coefficient $\kappa$ on concentration and temperature profile for the non-isothermal case ($\Delta H_A = -10\ kJ/mol$). Inner zone injection and parameters of the Table 1 are considered.

$$\frac{\partial c_1}{\partial \tau} = -\frac{\partial c_1}{\partial x} + \frac{1}{Pe_{z,M}}\frac{\partial^2 c_1}{\partial x^2} + \frac{1}{Pe_{\rho,M}}\left[\frac{\partial^2 c_1}{\partial \rho^2} + \frac{1}{\rho}\frac{\partial c_1}{\partial \rho}\right] - F\kappa\left(q_1^* - q_1\right), \tag{8}$$

$$\frac{\partial c_2}{\partial \tau} = -\frac{\partial c_2}{\partial x} + \frac{1}{Pe_{z,H}}\frac{\partial^2 c_2}{\partial x^2} + \frac{1}{Pe_{\rho,H}}\left[\frac{\partial^2 c_2}{\partial \rho^2} + \frac{1}{\rho}\frac{\partial c_2}{\partial \rho}\right] - F\beta_L(c_2 - q_2), \tag{9}$$

$$\frac{\partial q_1}{\partial \tau} = \kappa\left(q_1^* - q_1\right), \tag{10}$$

$$\frac{\partial q_2}{\partial \tau} = \frac{-\Delta H_A}{c_e}\kappa\left(q_1^* - q_1\right) + \beta_s(c_2 - q_2). \tag{11}$$

By considering small changes in the temperature and concentration, Eq. (5) can be expanded through Taylor expansion up to first order. Resultantly, the equilibrium relation between the stationary and mobile absorbed phases is linearizes as:

$$q_1^* \simeq q_1^*\left(c_{1,ref}, T_{ref}\right) + \left.\frac{\partial q_1^*}{\partial T_s}\right|_{\left(c_{1,ref},T_{ref}\right)}\left(T_s - T_{ref}\right) + \left.\frac{\partial q_1^*}{\partial c_1}\right|_{\left(c_{1,ref},T_{ref}\right)}\left(c_1 - c_{1,ref}\right), \tag{12}$$

where $c_{1,ref}$ denotes the reference concentration and $T_{ref}$ is the corresponding reference temperature. On using Eqs. (5) and (6) in Eq. (18), we get

$$q_1^*(c_1, q_2) = H_1 c_1 + H_2 q_2, \tag{13}$$

where $H_1 = a_{ref}$ and $H_2 = \frac{\Delta H_A c_{1,ref}}{R_g T_{ref}}$. The initial conditions are given as

$$c_1(x,\rho,0) = c_{1,init}, \quad q_1(x,\rho,0) = q_{1,init},$$

$$c_2(x,\rho,0) = c_{2,init}, \quad q_2(x,\rho,0) = q_{2,init}. \tag{14}$$

Here, $c_{2,init} = T_{init} - T_{ref}$ with $T_{init}$ being the initial temperature, $c_{1,init}$ stands for the initial concentration in the column, while $q_{1,init}$ and $q_{2,init}$ represent the initial concentration and temperature in the solid phase. Furthermore, different inflow conditions are assumed at the column inlet as elaborated below.

The inner circular region injection is stated as

$$c_1(x=0,\rho,\tau) = \begin{cases} c_{1,inj}, & \text{if} \quad 0 \le \tau \le \tau_{\text{inj}} \quad \text{and} \quad 0 \le \rho \le \tilde{\rho}, \\ 0, & \text{if} \quad \tau > \tau_{\text{inj}} \quad \text{or} \quad \tilde{\rho} < \rho \le 1, \end{cases} \tag{15a}$$

$$c_2(x=0,\rho,\tau) = \begin{cases} c_{2,inj}, & \text{if} \quad 0 \le \tau \le \tau_{\text{inj}} \quad \text{and} \quad 0 \le \rho \le \tilde{\rho}, \\ 0, & \text{if} \quad \tau > \tau_{\text{inj}} \quad \text{or} \quad \tilde{\rho} < \rho \le 1, \end{cases} \tag{15b}$$

where $\tilde{\rho} = \tilde{r}/R$. While, injection in the outer annular zone is stated as

$$c_1(x=0,\rho,\tau) = \begin{cases} c_{1,inj}, & \text{if} \quad 0 \le \tau \le \tau_{\text{inj}} \quad \text{and} \quad \tilde{\rho} < \rho \le 1, \\ 0, & \text{if} \quad \tau > \tau_{\text{inj}} \quad \text{or} \quad 0 \le \rho \le \tilde{\rho}, \end{cases} \tag{15c}$$

$$c_2(x=0,\rho,\tau) = \begin{cases} c_{2,inj}, & \text{if} \quad 0 \le \tau \le \tau_{\text{inj}} \quad \text{and} \quad \tilde{\rho} < \rho \le 1, \\ 0, & \text{if} \quad \tau > \tau_{\text{inj}} \quad \text{or} \quad 0 \le \rho \le \tilde{\rho}. \end{cases} \tag{15d}$$

To express injection via the whole inlet cross-section of the column, either set $\tilde{\rho} = 1$ in Eqs. (15a) and (15b) or set $\tilde{\rho} = 0$ in Eqs. (15c) and (15d).

Considering a column of hypothetically infinite length, conditions at the exit of the column are expressed as:

$$\left.\frac{\partial c_i(x,\rho,\tau)}{\partial x}\right|_{x=\infty} = 0, \quad i = 1,2. \tag{15e}$$

Here

$$c_{2,inj} = T_{inj} - T_{ref} \quad \text{and} \quad \tau_{inj} = \frac{u t_{inj}}{L}. \tag{16}$$

In the conditions above $c_{1,inj}$ expresses concentration of the injected component, $T_{inj}$ donates the temperature of injected component and $\tau_{inj}$ is the time of injection. In most of the liquid chromatographic operations, the Peclet numbers of energy and mass are sufficiently large (or axial heat conductivity and axial-dispersion coefficients are sufficiently small), providing a justification for the use of current simplified Dirichlet boundary conditions.

## Analytical solutions

The aforementioned linearized non-equilibrium and non-isothermal two-dimensional LKM is solved analytically by using the methods of Hankel and Laplace transformations. A zeroth-order Hankel transform of the $c(x,\rho,\tau)$ is defined as [46–48]

$$c_H(x,\lambda_n,\tau) = \mathcal{H}[c(x,\rho,\tau)] = \int_0^1 \big(c(x,\rho,\tau) J_0(\lambda_n \rho)\rho\big) d\rho, \tag{17a}$$

while, the inverse of the Hankel transform is stated as

$$c(x,\rho,\tau) = 2\left[c_H(x,\lambda_n=0,\tau) + \sum_{n=1}^{\infty} c_H(x,\lambda_n,\tau)\left(\frac{J_0(\lambda_n\rho)}{|J_0(\lambda_n)|^2}\right)\right]. \tag{17b}$$

On the other hand, the Laplace transformation of $c_H(x,\lambda_n,\tau)$ is expressed as [48]

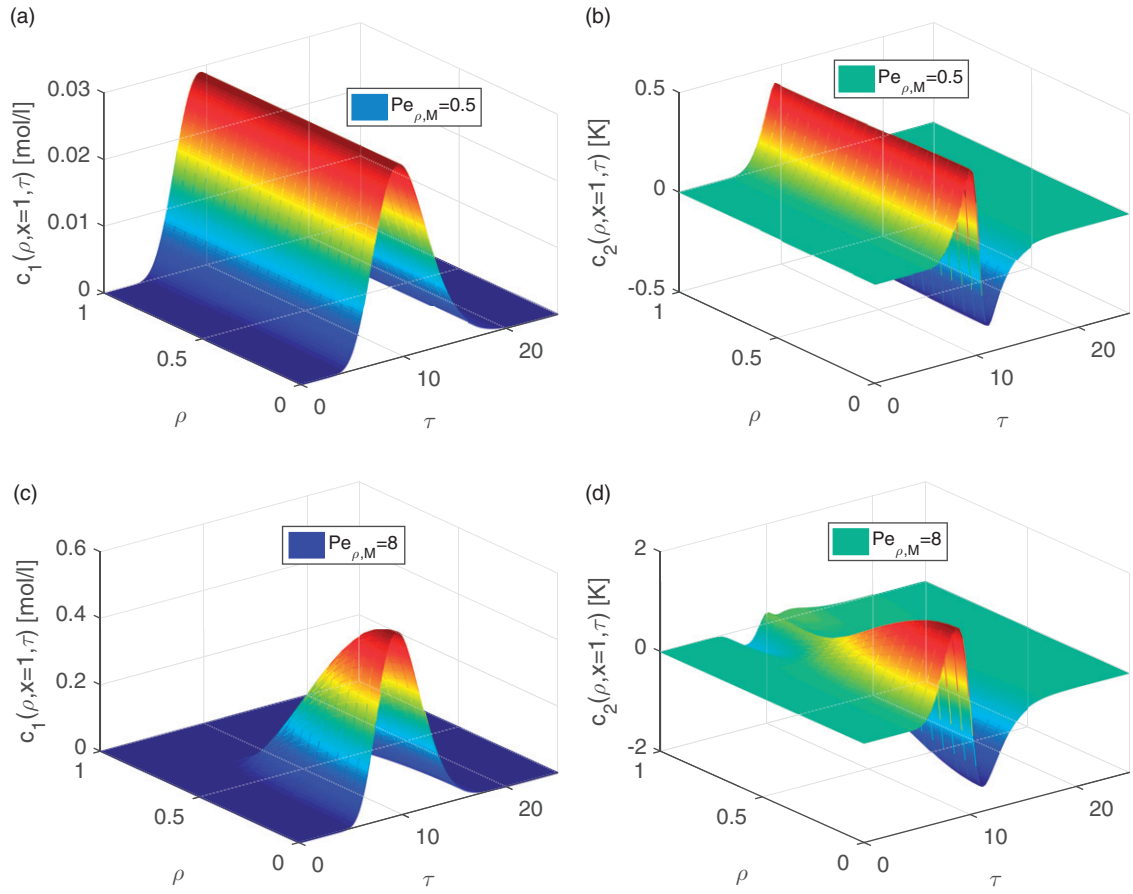


**Figure 7.** Effect of $Pe_{\rho,M}$ on concentration and temperature profiles for the non-isothermal case ($\Delta H_A = -10\ kJ/mol$). Here, plots for $Pe_{\rho,M} = 0.5$ are shown in (a) & (b), while plots for $Pe_{\rho,M} = 8$ are given in (c) & (d) assuming $\frac{\epsilon_e}{\epsilon_t} = 1$.

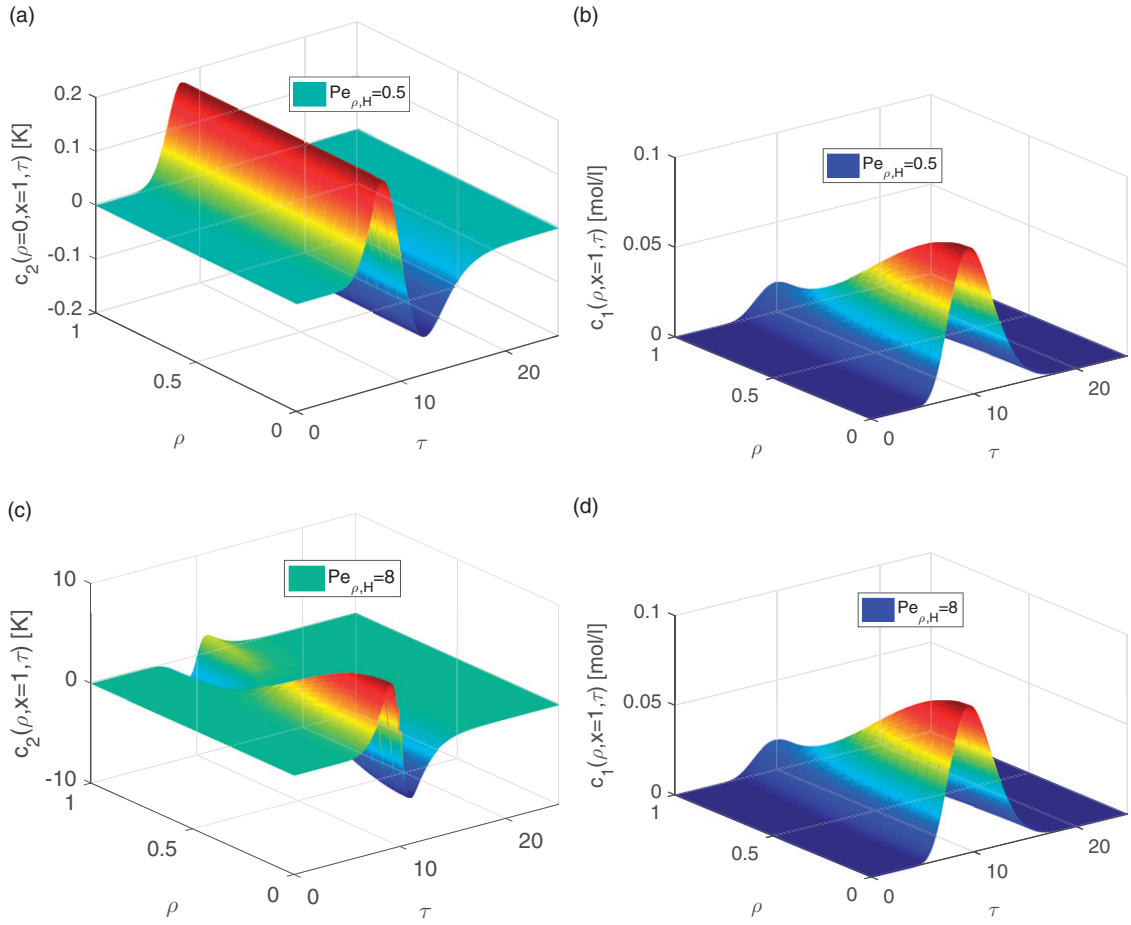


**Figure 8.** Effect of $Pe_{\rho,H}$ on concentration and temperature profiles for the non-isothermal case ($\Delta H_A = -10\ kJ/mol$). Here, plots for $Pe_{\rho,H} = 0.5$ are shown in (a) & (b), while plots for $Pe_{\rho,H} = 8$ are given in (c) & (d) assuming $\frac{c_e}{c_f} = 1$.

$$\bar{c}_H(x,\lambda_n,s) = \int_0^\infty \left[e^{-st} c_H(\lambda_n,x,\tau)\right] dt. \quad t \geq 0. \tag{17c}$$

Now, the above-mentioned transformations are applied on Eqs. (8)-(11) to solve them analytically. After applying these transformations and plugging the values of $q_1(s)$ and $q_2(s)$, the resulting equations have the forms

$$\frac{1}{Pe_{z,M}}\frac{\partial \bar{c}_{1,H}}{\partial x^2} - \frac{\partial \bar{c}_{1,H}}{\partial x} = \eta_1(s,\lambda_n)s\bar{c}_{1,H} - \eta_1(s,\lambda_n)sc_{1,int} + \alpha_2(s)s\bar{c}_{2,H}, \tag{18}$$

$$\frac{1}{Pe_{z,H}}\frac{\partial \bar{c}_{2,H}}{\partial x^2} - \frac{\partial \bar{c}_{2,H}}{\partial x} = \beta_1(s)s\bar{c}_{2,H} - \beta_1(s)c_{1,int} + \eta_2(s,\lambda_n)s\bar{c}_{2,H}, \tag{19}$$

where, the new parameters introduced in Eqs. (18) and (19) are defined as

$$\alpha_1(s) = 1 + \frac{F\kappa H_1}{s+\kappa} - \frac{F\Delta H_A \kappa^2 H_1 H_2 s}{c_e(s+\kappa)^2(s+\beta_s) + s(s+\kappa)\Delta H_A \kappa H_2},$$

$$\alpha_2(s) = \frac{F\beta_s c_e \kappa H_2}{c_e(s+\kappa)(s+\beta_s) + s\Delta H_A \kappa H_2},$$

$$\beta_1(s) = \frac{F\beta_L c_e \kappa H_2}{c_e(s+\kappa)(s+\beta_s) + s\Delta H_A \kappa H_2},$$

$$\beta_2(s) = 1 - \frac{F\beta_L c_e(s+\kappa) + \Delta H_A \kappa H_1 H_2 s}{c_e(s+\kappa)^2(s+\beta_s) + s(s+\kappa)\Delta H_A \kappa H_2},$$

$$\eta_1(s,\lambda_n) = \alpha_1(s) + \frac{\lambda_n^2}{sPe_{\rho,M}},\ \eta_2(s,\lambda_n) = \beta_2(s) + \frac{\lambda_n^2}{sPe_{\rho,H}}. \tag{20}$$

Eqs. (18) and (19) are written in compact form as

$$\begin{pmatrix} \frac{1}{Pe_{z,M}} \\ \frac{1}{Pe_{z,H}} \end{pmatrix} \frac{\partial^2}{\partial x^2}\begin{pmatrix} \bar{c}_{1,H} \\ \bar{c}_{2,H} \end{pmatrix} - \frac{\partial}{\partial x}\begin{pmatrix} \bar{c}_{1,H} \\ \bar{c}_{2,H} \end{pmatrix}$$

$$= \begin{pmatrix} \eta_1(s,\lambda_n) & \alpha_2(s) \\ \beta_1(s) & \eta_2(s,\lambda_n) \end{pmatrix}\begin{pmatrix} s\bar{c}_{1,H} - c_{1,init} \\ s\bar{c}_{2,H} \end{pmatrix}. \tag{21}$$

The matrix of the coefficients has the form

$$A = \begin{pmatrix} \eta_1(s,\lambda_n) & \alpha_2(s) \\ \beta_1(s) & \eta_2(s,\lambda_n) \end{pmatrix}. \tag{22}$$

The next step will be to decouple the above system by using the eigen-decomposition method. The above matrix

has two distinct eigenvalues, allowing its diagonalization. These eigenvalues are given as

$$\lambda_{1,2} = \frac{1}{2}[(\eta_1(s,\lambda_n) + \eta_2(s,\lambda_n)) \pm \sqrt{(\eta_1(s,\lambda_n) - \eta_2(s,\lambda_n))^2 + 4\alpha_2(s)\beta_1(s)}]. \quad (23)$$

The two associated eigenvectors are expressed as

$$x_1 = \begin{pmatrix} \lambda_1 - \eta_2(s,\lambda_n) \\ \beta_1(s) \end{pmatrix}, \quad x_2 = \begin{pmatrix} \lambda_2 - \eta_2(s,\lambda_n) \\ \beta_1(s) \end{pmatrix}. \quad (24)$$

On the basis of the above eigenvalues, the transformation Matrix B can be written as

$$B = \begin{pmatrix} \eta_1(s,\lambda_n) & \alpha_2(s) \\ \beta_1(s) & \eta_2(s,\lambda_n) \end{pmatrix}. \quad (25)$$

The following linear transformation is constructed by utilizing the transformation matrix B:

$$\begin{pmatrix} \bar{c}_{1,H} \\ \bar{c}_{2,H} \end{pmatrix} = \begin{pmatrix} \lambda_1 - \eta_2(s,\lambda_n) & \lambda_2 - \eta_2(s,\lambda_n) \\ \beta_1(s) & \beta_1(s) \end{pmatrix} \begin{pmatrix} \bar{\gamma}_1 \\ \bar{\gamma}_2 \end{pmatrix}. \quad (26)$$

By implementing the above transformation on the system in Eq. (21), we obtain

$$\frac{1}{Pe_{z,M}}\frac{d^2\bar{\gamma}_1}{dx^2} - \frac{d\bar{\gamma}_1}{dx} - s\lambda_1\bar{\gamma}_1 = -\lambda_1\gamma_{1,init}, \quad (27)$$

$$\frac{1}{Pe_{z,H}}\frac{d^2\bar{\gamma}_2}{dx^2} - \frac{d\bar{\gamma}_2}{dx} - s\lambda_2\bar{\gamma}_2 = -\lambda_2\gamma_{2,init}, \quad (28)$$

where

$$\gamma_{1,init} = \frac{c_{1,init}}{\lambda_1 - \lambda_2}, \quad \gamma_{2,init} = -\frac{c_{1,init}}{\lambda_1 - \lambda_2}. \quad (29)$$

The two Eqs. (27) and (28) describe decoupled steady-state of advection-dispersion equations. Our focus is to determined the analytical solutions these two separated equations. The solutions of Eq. (27) is

$$\bar{\gamma}_1(x,\lambda_n,s) = \mathcal{A}_1 e^{a_1 x} + \mathcal{B}_1 e^{a_2 x} + \frac{\gamma_{1,init}}{s}, \quad (30)$$

where

$$a_{1,2} = Pe_{z,M} \pm \sqrt{Pe_{z,M}^2 + 4sPe_{z,M}\lambda_1}. \quad (31)$$

In a similar manner, the solution of Eq. (28) is obtained as

$$\bar{\gamma}_2(x,\lambda_n,s) = \mathcal{A}_2 e^{b_1 x} + \mathcal{B}_2 e^{b_2 x} + \frac{\gamma_{2,init}}{s}, \quad (32)$$

where

$$b_{1,2} = Pe_{z,H} \pm \sqrt{Pe_{z,H}^2 + 4sPe_{z,H}\lambda_2}. \quad (33)$$

The constants of integrations appearing in Eq. (27) and (28), i.e. $\mathcal{A}_1, \mathcal{A}_2, \mathcal{B}_1$ and $\mathcal{B}_2$, are evaluated by means of the

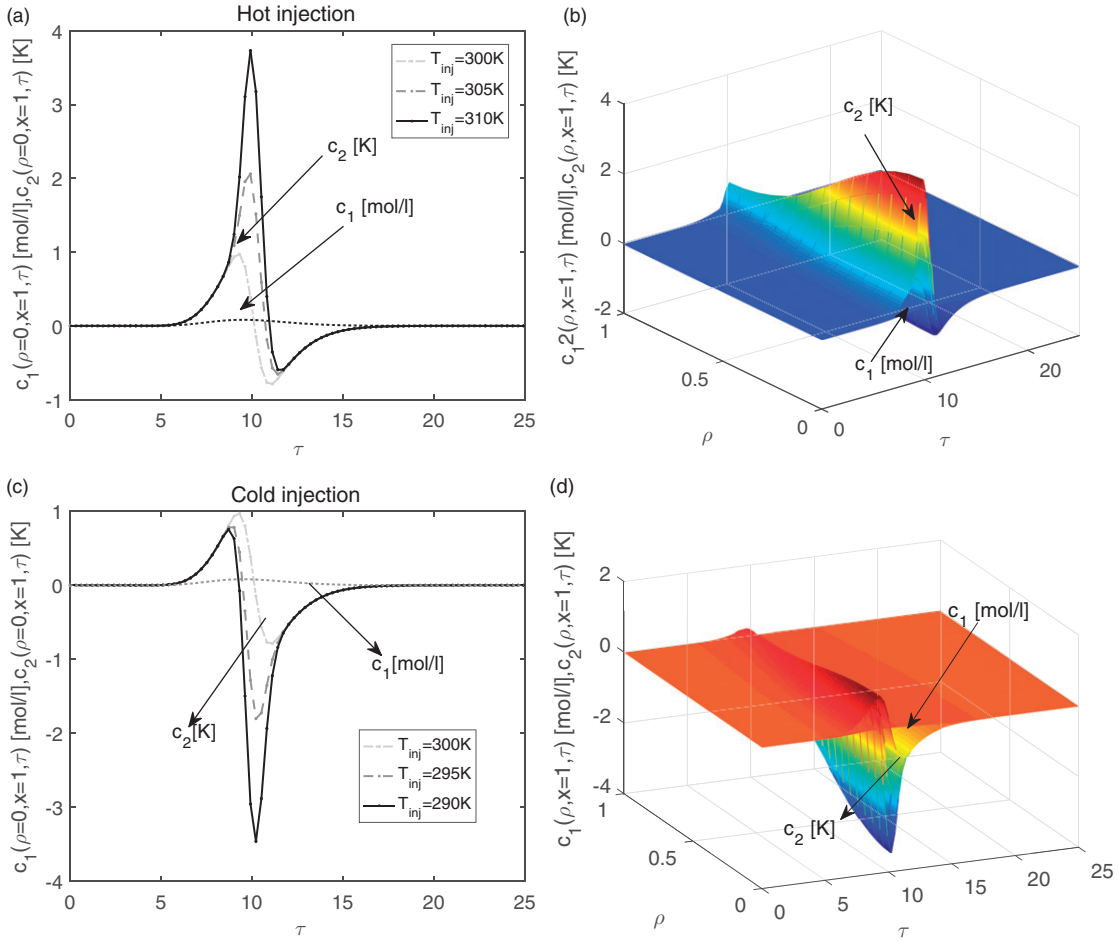


**Figure 9.** Effect of injected temperature $T_{inj}$ on concentration and temperature profiles considering $\Delta H_A = -10\ kJ/mol$, $\frac{c_e}{c_f} = 1$ and inner zone injection.

considered two different sets of boundary of conditions (BCs). By applying the Hankel transforms on Eqs. (17a) (or (17 b)) and (17c), the following equations are obtained

$$c_{i,H}(x,\lambda_n,\tau)=\begin{cases} c_{i,inj}\mathcal{F}(\lambda_n), & \text{if} \quad 0\le\tau\le\tau_{\text{inj}},\\ 0, & \text{if} \quad \tau>\tau_{\text{inj}},\end{cases} \tag{34a}$$

$$\left.\frac{\partial c_{i,H}(x,\lambda_n,\tau)}{\partial x}\right|_{x=\infty}=0, \quad i=1,2. \tag{34b}$$

Here $\mathcal{F}(\lambda_n)$ for the inner cylindrical core injection is given as

$$\mathcal{F}(\lambda_n)=\begin{cases}\dfrac{\tilde{\rho}^2}{2}, & \text{if} \quad \lambda_n=0,\\ J_1(\lambda_n\tilde{\rho})\dfrac{\tilde{\rho}}{\lambda_n}, & \text{if} \quad \lambda_n\neq 0.\end{cases} \tag{34c}$$

While, for the case of outer annular ring injection, $F(\lambda_n)$ is stated as

$$\mathcal{F}(\lambda_n)=\begin{cases}\left(\dfrac{1}{2}-\dfrac{\tilde{\rho}^2}{2}\right), & \text{if} \quad \lambda_n=0,\\ -J_1(\lambda_n\tilde{\rho})\dfrac{\tilde{\rho}}{\lambda_n}, & \text{if} \quad \lambda_n\neq 0.\end{cases} \tag{34d}$$

After applying the Laplace transformation on Eqs. (34a) and (34b), the equations below were obtained

$$\bar{c}_{i,H}(x,\lambda_n,s)=\frac{\mathcal{F}(\lambda_n)}{s}c_{i,inj}(1-e^{-s\tau_{\text{inj}}}),$$

$$\left.\frac{\partial\bar{c}_{i,H}}{\partial x}\right|_{x=\infty}=0, \quad i=1,2. \tag{35}$$

In $\bar{\gamma}$ domain, the above transformations take the forms

$$\bar{\gamma}_{1,H}(0,s,\lambda_n)=\frac{(1-e^{-s\tau_{inj}})\mathcal{F}(\lambda_n)}{s\beta_1(s)(\lambda_1-\lambda_2)}$$

$$\left[\beta_1(s)c_{1,inj}-(\lambda_2-\eta_2(s,\lambda_n))c_{2,inj}\right], \tag{36a}$$

$$\bar{\gamma}_{2,H}(0,s,\lambda_n)=\frac{(1-e^{-s\tau_{inj}})\mathcal{F}(\lambda_n)}{s\beta_1(s)(\lambda_2-\lambda_2)}$$

$$\left[\beta_1(s)c_{1,inj}-(\lambda_1-\eta_2(s,\lambda_n))c_{2,inj}\right], \tag{36b}$$

where

$$\left.\frac{d\bar{\gamma}_{i,H}}{dx}\right|_{x=\infty}=0, \quad i=1,2. \tag{37}$$

Using Eqs. (36a) and (36b), the constants of the integration $\mathcal{A}_1,\mathcal{A}_2,\mathcal{B}_1$ and $\mathcal{B}_2$ have the following values

$$\mathcal{A}_1=0, \quad \mathcal{A}_2=0, \quad \mathcal{B}_1=\bar{\gamma}_{1,H}(0,s,\lambda_n)-\frac{\gamma_{1,init}}{s},$$

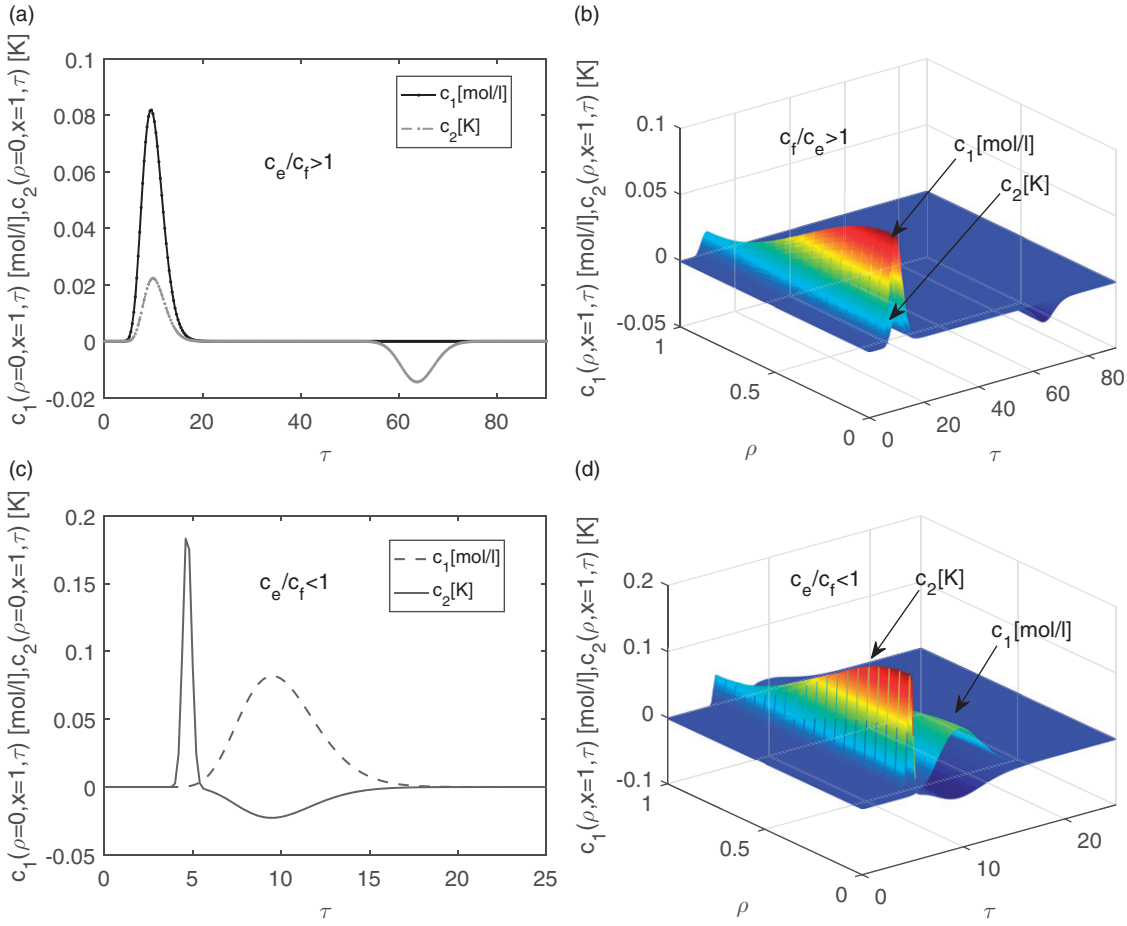


**Figure 10.** Effect of density times heat capacity ratio of solid and liquid phases $\frac{c_e}{c_f}$ on concentration and temperature profiles. For plots (a) & (b): $c_e=40$ and $c_f=4$, while for plots (c) & (d): $c_e=4$ and $c_f=40$. Here, $\Delta H_A=-10\ kJ/mol$ and inner zone injection are considered.

$$\mathcal{B}_2 = \bar{\gamma}_{2,H}(0,s,\lambda_n) - \frac{\gamma_{2,init}}{s}. \tag{38}$$

On substituting $\mathcal{A}_1$ and $\mathcal{B}_1$ values in Eq. (30), and $\mathcal{A}_2$ and $\mathcal{B}_2$ values in Eq. (32), we obtain

$$\bar{\gamma}_{1,H}(x,s,\lambda_n) = \frac{(1-e^{-s\tau_{inj}})\mathcal{F}(\lambda_n)}{s\beta_1(s)(\lambda_1-\lambda_2)}\left[\beta_1(s)c_{1,inj} - (\lambda_2-\eta_2(s,\lambda_n))c_{2,inj}\right] \times e^{a_2 x} + \frac{\gamma_{1,init}}{s}(1-e^{a_2 x}), \tag{39}$$

$$\bar{\gamma}_{2,H}(x,s,\lambda_n) = \frac{(1-e^{-s\tau_{inj}})\mathcal{F}(\lambda_n)}{s\beta_1(s)(\lambda_2-\lambda_2)}\left[\beta_1(s)c_{1,inj} - (\lambda_1-\eta_2(s,\lambda_n))c_{2,inj}\right] \times e^{b_2 x} + \frac{\gamma_{1,init}}{s}(1-e^{b_2 x}). \tag{40}$$

After utilizing the transformation in Eq. (26), the final Hankel-Laplace domains solutions are obtained as

$$\bar{c}_{1,H}(x,\lambda_n,s) = \frac{(1-e^{-s\tau_{inj}})c_{1,inj}\mathcal{F}(\lambda_n)}{(\lambda_1-\lambda_4)s}\left[(\lambda_1-\eta_2(s,\lambda_n))e^{a_2 x} - (\lambda_2-\eta_2(s,\lambda_n))e^{b_2 x}\right] + \frac{(1-e^{-s\tau_{inj}})c_{2,inj}\mathcal{F}(\lambda_n)(\lambda_2-\eta_2(s,\lambda_n))(\lambda_1-\eta_2(s,\lambda_n))}{\beta_1(s)(\lambda_1-\lambda_2)s}\left[e^{a_2 x} - e^{b_2 x}\right], \tag{41}$$

$$\bar{c}_{2,H}(x,\lambda_n,s) = \frac{(1-e^{-s\tau_{inj}})\beta_1(s)c_{1,inj}\mathcal{F}(\lambda_n)}{(\lambda_1-\lambda_2)s}\left[e^{a_2 x} - e^{b_2 x}\right] + \frac{(1-e^{-s\tau_{inj}})c_{2,inj}\mathcal{F}(\lambda_n)}{(\lambda_1-\lambda_2)s}\left[(\lambda_2-\eta_2(s,\lambda_n))e^{a_2 x} - (\lambda_1-\eta_2(s,\lambda_n))e^{b_2 x}\right]. \tag{42}$$

The analytical Hankel and Laplace inversions of Eqs. (41) and (42) are not attainable. For that reason, the numerical Hankel and Laplace inversions are employed to get accurate solutions in the existing time domain [36–38,43].

## Numerical test cases

Various case studies are conducted to examine the behavior of analytical solutions. To access the validity ranges of our analytical solutions, a high-resolution finite volume scheme (HR-FVS) is also applied to numerically approximate the full nonlinear model equations considering the isotherm in Eq. (5) [49]. The numerical test cases also explain the coupling between the concentration and thermal fronts. In the analytical solutions, the linearized isotherm is considered

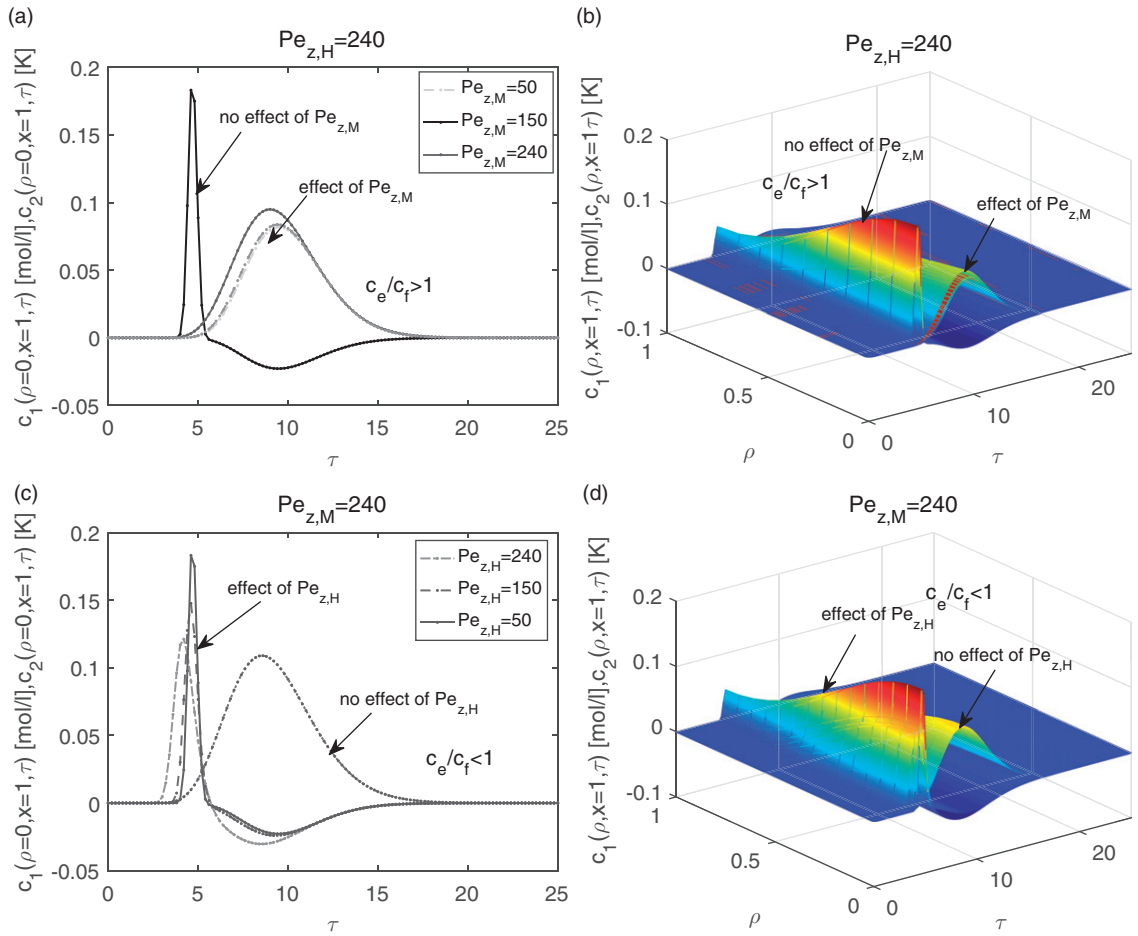


**Figure 11.** Influence of axial Peclet numbers on concentration and temperate profiles considering ($\Delta H_A = -10\ kJ/mol$), $\frac{c_e}{c_f} < 1$ and inner zone injection.

with a Henry's constant $a_{ref} = 1.0$ at a reference temperature $T_{ref} = 300\,\mathrm{K}$. A column of length $L = 4.0\,\mathrm{cm}$ is considered and the interstitial velocity is taken as $u = 1.5\,\mathrm{cm/min}$. The values of axial and radial dispersion coefficients for the concentration in the bulk phase are chosen in a manner to produce Peclet numbers of $Pe_{z,M} = 240$ and $Pe_{\rho,M} = 6$, while their values for energy in the bulk phase have generated $Pe_{z,H} = 240$ and $Pe_{\rho,H} = 6$. All other parameters are stated in Table 1 and their values are selected from the typical ranges encountered in high-performance liquid chromatography (HPLC) applications.

## Effect of adsorption enthalpy $\Delta H_A$

Figures 2 and 3 display the isothermal and non-isothermal solutions for inner zone injection. It is evident from Figure 2 that isothermal operating condition ($\Delta H_A = 0\,\mathrm{kJ/mol}$) produces no effect on the temperature profile, leading to a steady state temperature profile (c.f. see Figure 2). On the other hand, the non-isothermal operating condition ($\Delta H_A = -10\,\mathrm{kJ/mol}$) produces visible temperature fluctuations as shown in Figure 3. Because of the considered linearity and low amplitudes of temperature variations, the concentration profile is not effected by such temperature variations. Due to inner zone injection, the values of concentration and temperature are larger in the inner region of the column (c.f. Figure 3b and Figure 3d). Due to larger values of radial Peclet numbers (or small values of radial dispersion coefficients), variations in the profiles along the radial coordinate of the column are visible in Figure 2 and Figure 3. Also, Figure 4 displays the non-isothermal case results for the outer zone injection. Now, the profiles have higher values in the outer annular region of the column, while other effects are similar. Lastly, Figure 5 compares the analytical results for linearized isotherm and numerical results for the nonlinear isotherm for two different values of $\Delta H_A$. It is evident from the figure that analytical and numerical solutions are similar for small magnitude of $\Delta H_A$, while they are deviating from each other for larger value of $\Delta H_A$. It is also observed that our analytical solutions are producing over-predicting results. These observations clearly endorse our assumptions for linearization.

## *Effect of mass transfer coefficient $\kappa$*

Figure 6 displays the results for three different values of $\kappa$ and for injection in the inner region. It is noticed that broadened profiles are generated for smaller value of $\kappa$, while they become sharper when the value of $\kappa$ is increased.

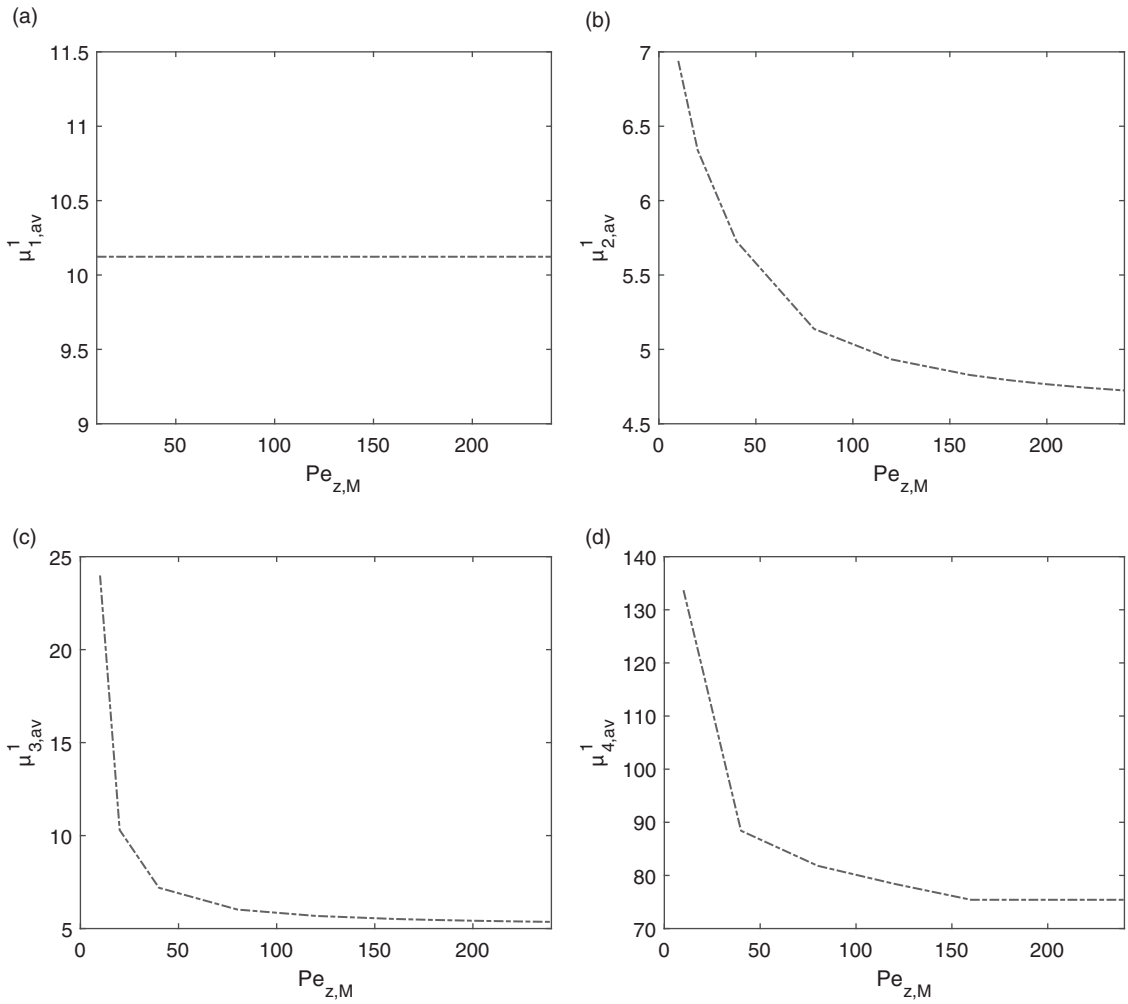


**Figure 12.** Effect of the axial Peclet number ($Pe_{z,M}$) on the averaged concentration monuments considering ($\Delta H_A = -10\ kJ/mol$) and inner zone injection.

For sufficiently larger value of $\kappa$, i.e. $\kappa \geq 267$, the results of current LKM reduces to those of simplified EDM.

### Effects of radial peclet numbers

Figures 7 and 8 displays the effects of $Pe_{\rho,M}$ and $Pe_{\rho,H}$ on the temperature and concentration profiles. It was found that $Pe_{\rho,H}$ influences the temperature profile only, while $Pe_{\rho,M}$ effects both the temperature and concentration profiles. For small values of radial Peclet numbers (or larger values of radial dispersion coefficients), no changes are seen in the profiles along the radial coordinate of the column.

### Effect of injection temperature $T_{ref} \neq T_{inj}$

The effect of injected temperature is analyzed on the concentration and temperature profiles in Figure 9. A rise in the injected temperature enlarges the adsorption peak of temperature, while reducing the desorption peak (c.f. Figure 9a,b). The injected temperature lower than the reference temperature minimizes the adsorption peaks and enlarges the desorption peak downward (c.f. Figure 9c,d).

### Effect of ratio $\frac{c_e}{c_f}$

The effect ratio of $\frac{c_e}{c_f}$ is shown in Figure 10. For $\frac{c_e}{c_f}>1$, the velocity of temperature profile is lower than the concentration profile in Figure 10a,b. In this case, the faster concentration peak is coupled with the adsorption peak of temperature. On the other hand, the desorption peak of temperature, which is slow and decoupled, exits the column at a later time. Contrarily, for $\frac{c_e}{c_f}<1$, the velocity of concentration profile is lower than the temperature profile as shown in Figure 10c,d. In this case, the concentration peak is coupled with the desorption peak of temperature, while the adsorption peak of temperature is faster and decoupled. It was already observed in Figure 3 that, for the case $\frac{c_e}{c_f}=1$, both temperature and concentration profiles are moving at very similar speeds.

### Effects of axial peclet numbers

The precise effects of the two axial Peclet numbers of mass and heat transfer (i.e $Pe_{z,M}$ and $Pe_{z,H}$) on the concentration and temperature profiles are presented in Figure 11 for the value of ratio $\frac{c_e}{c_f}<1$ and $T_{inj} = T_{ref}$. In Figure 11a,b, the effect of $Pe_{z,M}$ is studied for a fixed value of $Pe_{z,M} = 240$. The variation of $Pe_{z,M}$ has a pronounced effect only if the

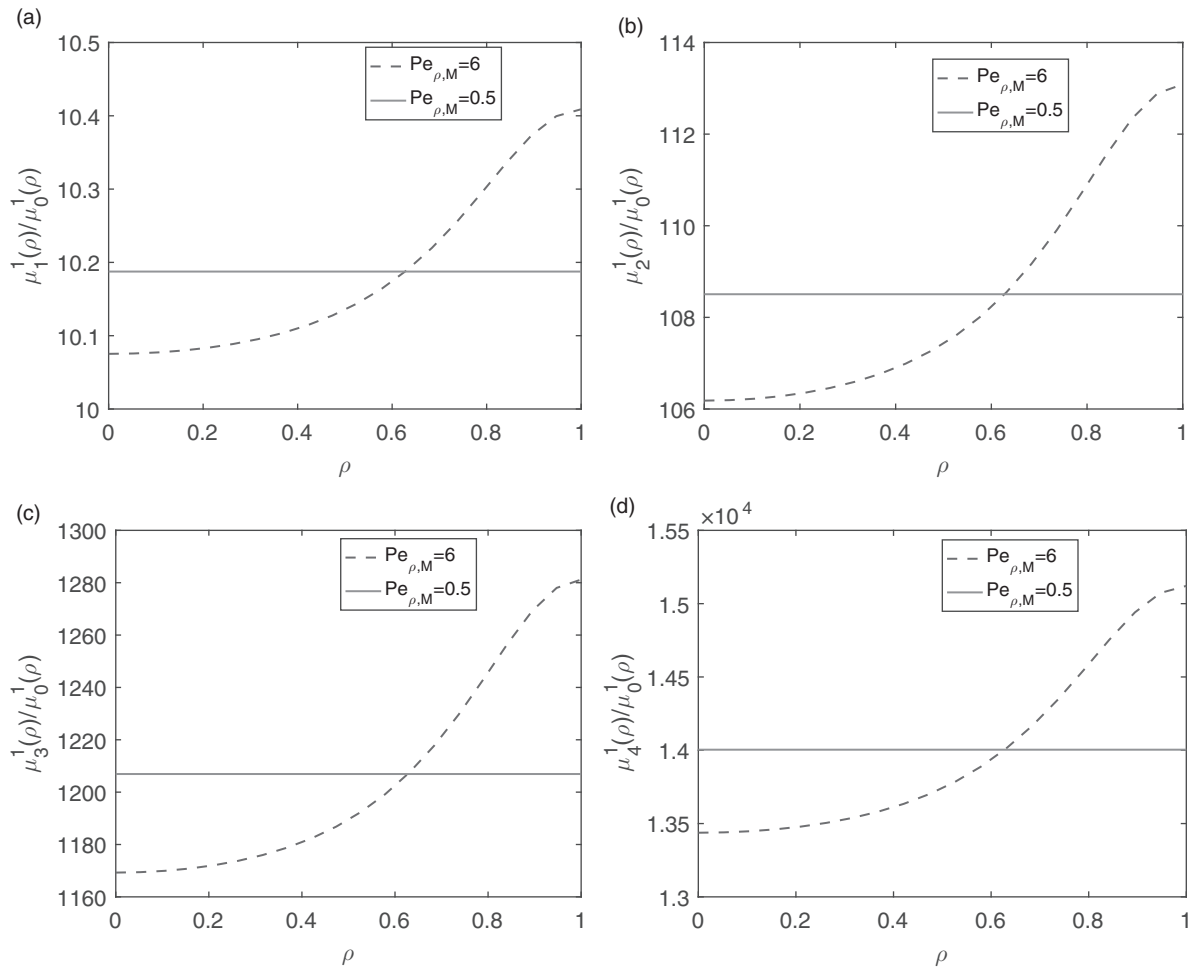


Figure 13. Effect of the radial Peclet number ($Pe_{\rho,M}$) on the radial concentration monuments considering ($\Delta H_A = -10\ kJ/mol$) and inner zone injection.

concentration and temperature peaks are coupled, while it has no effect on the separated decoupled temperature peak. The coupled peaks of concentration and temperature clearly become broader on decreasing the value of $Pe_{z,M}$. In contrast, Figure 11c,d shows the influence of $Pe_{z,H}$ (c.f. Figure 11c,d) on the concentration and temperature profiles for fixed $Pe_{z,M}$. It can be seen that $Pe_{z,H}$ only effects the decoupled temperature peaks, while it has no effect on the coupled concentration and temperature peaks. The decoupled temperature peaks become broadened on decreasing the value of $Pe_{z,H}$. Similarly the result for the value ratio $\frac{c_\alpha}{c_f} > 1$ is applicable in the same manner.

### Calculation and discussion of numerical moments

Here, the numerical moments are obtained up to the fourth order. The numerical radial moments at the column outlet ($x = 1$) are obtained as

$$\mu_k^j(\rho) = \int_0^\infty c_j(\rho, x = 1, \tau)\tau^k d\tau, \quad j = 1, 2, \quad k = 0, 1, 2, 3, 4. \tag{43}$$

The normalized averaged moments of the band profiles, averaged over the radial coordinate ($\rho$), are expressed as

$$\mu_{0,av}^j = \int_0^\infty c_{j,av}(x = 1, \tau)d\tau, \quad \mu_{k,av}^j = \frac{\int_0^\infty c_{j,av}(x = 1, \tau)\tau^k d\tau}{\mu_{0,av}^j}, \quad k = 1, 2, 3, 4, \tag{44}$$

where

$$c_{j,av} = 2\int_0^1 c_j(\rho, x = 1, \tau)\rho d\rho. \tag{45}$$

Now, the dimensionless moments are plotted to analyze the effects of axial and radial Peclet numbers for mass (i.e. $Pe_{z,M}$ and $Pe_{\rho,M}$) on the concentration profile using the solution for inner zone injection. Figure 12 displays the plots of concentration moments with respect to the axial Peclet number $Pe_{z,M}$, while keeping $Pe_{\rho,M}$ fixed. As expected, no effect of $Pe_{z,M}$ can be seen on the first moments. However, the second, third and fourth moments are decreasing on increasing the value of $Pe_{z,M}$ (or on decreasing the value of axial dispersion $D_z$). Finally, Figure 13 shows the plots of radial moments with respect to the radial coordinate $\rho$ for two different values of radial Peclet number $Pe_{\rho,M}$. For larger value of $Pe_{\rho,M}$ (or smaller smaller value of $D_\rho$), one can see changes in the radial moments along the radial coordinate. However, radial moments remain constant for smaller value of $Pe_{\rho,M}$ (or larger value of $D_\rho$). These results agree with those obtained in Figures 7 and 11.

## Conclusion

A linearized non-equilibrium and non-isothermal two-dimensional lumped kinetics model was formulated and solved analytically to study the influence of thermal variations on the liquid chromatographic process. The model equations comprise of partial differential equations coupled with differential and algebraic equations. The finite Hankel transform, the Laplace transform, the eigen-decomposition technique, and a conventional technique for the solutions of ODEs were jointly applied to obtain analytical solutions of the model for Dirichlet boundary conditions. The numerical inversion was employed to get solutions in the actual time domain, as analytical Hankel-Laplace inversions were not possible. These analytical solutions were used to deduce numerical moments of concentration profiles. These moments could be helpful to explore and investigate the process in more depth. The high-resolution finite volume technique was extended to solve the full nonlinear model numerically. The numerical solutions were used to verify the ranges of validity of our analytical results. The determined analytical solutions and numerical moments will be helpful to investigate and interpret mass and energy profiles in non-equilibrium and non-isothermal liquid chromatographic columns of cylindrical geometry without performing costly experiments in the laboratory.

## Funding

The first author is indebted to The World Academy of Sciences (TWAS) and COMSATS University Islamabad for the Award of 2016 CIIT-TWAS Full-time Postgraduate Fellowship [FR number: 3240293220].

## ORCID

Shamsul Qamar http://orcid.org/0000-0002-7358-6669

## References

[1] Guiochon, G.; Felinger, A.; Shirazi, D. G.; Katti, A. M. *Fundamentals of Preparative and Nonlinear Chromatography*, 2nd ed. Elsevier Academic Press: New York, **2006**.

[2] Miyabe, K.; Guiochon, G. Influence of the Modification Conditions of Alkyl Bonded Ligands on the Characteristics of Reversed-Phase Liquid Chromatography. *J. Chromatogr. A.* **2000**, *903*, 1–12. DOI: 10.1016/S0021-9673(00)00891-8.

[3] Miyabe, K.; Guiochon, G. Measurement of the Parameters of the Mass Transfer Kinetics in High Performance Liquid Chromatography. *J. Sep. Sci.* **2003**, *26*, 155–173. DOI: 10.1002/jssc.200390024.

[4] Ruthven, D. M. *Principles of Adsorption and Adsorption Processes*. Wiley-Interscience: New York, **1984**.

[5] Guiochon, G. Preparative Liquid Chromatography. *J. Chromatogr. A.* **2002**, *965*, 129–161.

[6] Qamar, S.; Sattar, F. A.; Batool, I.; Seidel-Morgenstern, A. Theoretical Analysis of the Influence of Forced and Inherent Temperature Fluctuations in an Adiabatic Chromatographic Column. *Chem. Eng. Sci.* **2017**, *161*, 249–264. DOI: 10.1016/j.ces.2016.12.027.

[7] Brandt, A.; Mann, G.; Arlt, W. Temperature Gradients in Preparative High-Performance Liquid Chromatography Columns. *J. Chromatogr. A.* **1997**, *769*, 109–117. DOI: 10.1016/S0021-9673(97)00235-5.

[8] Javeed, S.; Qamar, S.; Ashraf, W.; Warnecke, G.; Seidel-Morgenstern, A. Analysis and Numerical Investigation of Two Dynamic Models for Liquid Chromatography. *Chem. Eng. Sci.* **2013**, *90*, 17–31. DOI: 10.1016/j.ces.2012.12.014.

[9] Sainio, T.; Kaspereit, M.; Kienle, A.; Seidel-Morgenstern, A. Thermal Effects in Reactive Liquid Chromatography. *Chem. Eng. Sci.* **2007**, *62*, 5674–5681. DOI: 10.1016/j.ces.2007.02.033.

[10] Sainio, T.; Zhang, L.; Seidel-Morgenstern, A. Adiabatic Operation of Chromatographic Fixed-Bed Reactors. *Chem. Eng. J.* **2011**, *168*, 861–871. DOI: 10.1016/j.cej.2011.02.010.

[11] Haynes, H. W. Jr.; An Analysis of Sorption Heat Effects in the Pulse Gas Chromatography Diffusion Experiment. *AIChE J.* **1986**, *32*, 1750–1753. DOI: 10.1002/aic.690321021.

[12] Guillaume, Y.; Guinchard, C. Prediction of Retention Times, Column Efficiency, and Resolution in Isothermal and Temperature-Programmed Gas Chromatography: Application for Separation of Four Psoalens. *J. Chromatogr. Sci.* **1997**, *35*, 14–18. DOI: 10.1093/chromsci/35.1.14.

[13] Xiu, G.; Li, P.; Rodrigues, A. E. Sorption-Enhanced Reaction Process with Reactive Regeneration. *Chem. Eng. Sci.* **2002**, *57*, 3893–3908. DOI: 10.1016/S0009-2509(02)00245-2.

[14] Peter, G. R.; Allan, L. O. Comparison of Isothermal and Non-Linear Temperature Programmed Gas Chromatography the Temperature Dependence of the Retention Indices of a Number of Hydrocarbons on Squalane and SE-30. *J. Chromatogr. A.* **1971**, *57*, 11–17. DOI: 10.1016/0021-9673(71)80002-X.

[15] Kaczmarski, K.; Gritti, F.; Guiochon, G. Prediction of the Influence of the Heat Generated by Viscous Friction on the Efficiency of Chromatography Columns. *J. Chromatogr. A.* **2008**, *1177*, 92–104.

[16] Gritti, F.; Michel Martin, M.; Guiochon, G. Influence of Viscous Friction Heating on the Efficiency of Columns Operated under Very High Pressures. *Anal. Chem.* **2009**, *81*, 3365–3384. DOI: 10.1021/ac802632x.

[17] Teutenberg, T. High-Temperature Liquid Chromatography: A User's Guide for Method Development. *RSC Chromatography Mon.* **2010**, *13*, 1–210.

[18] Horváth, C.; Melander, W.; Molnar, I. Solvophobic Interactions in Liquid Chromatography with Nonpolar Stationary Phases. *J. Chromatogr. A.* **1976**, *125*, 129–156. DOI: 10.1016/S0021-9673(00)93816-0.

[19] Antia, F. D.; Horvath, C. High-Performance Liquid Chromatography at Elevated Temperatures: Examination of Conditions for the Rapid Separation of Large Molecules. *J. Chromatogr. A.* **1988**, *435*, 1–15.

[20] Snyder, D. C.; Dolan, J. W. Initial Experiments in High-Performance Liquid Chromatographic Method Development I. Use of a Starting Gradient Run. *J. Chromatogr. A.* **1996**, *721*, 3–14. DOI: 10.1016/0021-9673(95)00770-9.

[21] Snyder, L. R.; Dolan, J. W.; Lommen, D. C. Drylab®Computer Simulation for High-Performance Liquid Chromatographic Method Development: I. Isocratic Elution. *J. Chromatogr. A.* **1989**, *485*, 45–89.

[22] Poppe, H. Some Reflections on Speed and Efficiency of Modern Chromatographic Methods. *J. Chromatogr. A.* **1997**, *778*, 3–21. DOI: 10.1016/S0021-9673(97)00376-2.

[23] Poppe, H.; Kraak, J. C.; Huber, J. F. K.; Van den Berg, J. H. M. Temperature Gradients in HPLC Columns Due to Viscous Heat Dissipation. *Chromatographia* **1981**, *14*, 515–523. DOI: 10.1007/BF02265631.

[24] Miyabe, K. Moment Analysis of Chromatographic Behavior in Reversed-Phase Liquid Chromatography. *J. Sep. Sci.* **2009**, *32*, 757–770. DOI: 10.1002/jssc.200800607.

[25] Suzuki, M.; Smith, J. M. Kinetic Studies by Chromatography. *Chem. Eng. Sci.* **1971**, *26*, 221–235. DOI: 10.1016/0009-2509(71)80006-4.

[26] Suzuki, M. Notes on Determining the Moments of the Impulse Response of the Basic Transformed Equations. *J. Chem. Eng. Japan./Jcej.* **1974**, *6*, 540–543. DOI: 10.1252/jcej.6.540.

[27] Lapidus, L.; Amundson, N. R. Mathematics of Adsorption in Beds. VI. The Effect of Longitudinal Diffusion in Ion Exchange and Chromatographic Columns. *J. Phys. Chem.* **1952**, *56*, 986–988.

[28] Eyring, H. The Activated Complex in Chemical Reactions. *J. Chem. Phys.* **1935**, *3*, 107–115. DOI: 10.1063/1.1749604.

[29] Schettler, P. D.; Giddings, J. C. New Method for Prediction of Binary Gas-Phase Diffusion Coefficients. *Ind. Eng. Chem.* **1966**, *58*, 18–27. DOI: 10.1021/ie50677a007.

[30] Qamar, S.; Sattar, F. A.; Abbasi, J. N.; Seidel-Morgenstern, A. Numerical Simulation of Nonlinear Chromatography with Core-Shell Particles Applying the General Rate Model. *Chem. Eng. Sci.* **2016**, *147*, 54–64. DOI: 10.1016/j.ces.2016.03.027.

[31] Qamar, S.; Bibi, S.; Khan, F. U.; Shah, M.; Javeed, S.; Seidel-Morgenstern, A. Irreversible and Reversible Reactions in a Liquid Chromatographic Column: Analytical Solutions and Moment Analysis. *Ind. eng. Chem. Res.* **2014**, *53*, 2461–2472. DOI: 10.1021/ie403645w.

[32] Bibi, S.; Qamar, S.; Seidel-Morgenstern, A. Irreversible and Reversible Reactive Chromatography: Analytical Solutions and Moment Analysis for Rectangular Pulse Injections. *J. Chromatogr. A.* **2015**, *1385*, 49–62. DOI: 10.1016/j.chroma.2015.01.065.

[33] Qamar, S.; Abbasi, J. N.; Javeed, S.; Shah, M.; Khan, F. U.; Seidel-Morgenstern, A. Analytical Solutions and Moment Analysis of Chromatographic Models for Rectangular Pulse Injections. *J. Chromatogr. A.* **2013**, *1315*, 92–106. DOI: 10.1016/j.chroma.2013.09.031.

[34] Qamar, S.; Abbasi, J.; Mehwish, A.; Seidel-Morgenstern, A. Linear General Rate Model of Chromatography for Core-Shell Particles: Analytical Solutions and Moment Analysis. *Chem. Eng. Sci.* **2015**, *137*, 352–363. DOI: 10.1016/j.ces.2015.06.053.

[35] Leweke, S.; von Lieres, E. Fast Arbitrary Order Moments and Arbitrary Precision Solution of the General Rate Model of Column Liquid Chromatography with Linear Isotherm. *Comput. Chem. Eng.* **2016**, *84*, 350–362. DOI: 10.1016/j.compchemeng.2015.09.009.

[36] Qamar, S.; Khan, F. U.; Mehmood, Y.; Seidel-Morgenstern, A. Analytical Solution of a Two-Dimensional Model of Liquid Chromatography Including Moment Analysis. *Chem. Eng. Sci.* **2014**, *116*, 576–589. DOI: 10.1016/j.ces.2014.05.043.

[37] Parveen, S.; Qamar, S.; Seidel-Morgenstern, A. Two-Dimensional Non-Equilibrium Model of Liquid Chromatography: Analytical Solutions and Moment Analysis. *Chem. Eng. Sci.* **2015**, *122*, 64–77. DOI: 10.1016/j.ces.2014.09.018.

[38] Parveen, S.; Qamar, S.; Seidel-Morgenstern, A. Analysis of Two-Dimensional Non-Equilibrium Model of Linear Reactive Chromatography considering Irreversible and Reversible Reactions. *Ind. Eng. Chem. Res.* **2016**, *55*, 2471–2482. DOI: 10.1021/acs.iecr.5b04714.

[39] Qamar, S.; Uche, D. U.; Khan, F. U.; Seidel-Morgenstern, A. Analysis of Linear Two-Dimensional General Rate Model for Chromatographic Columns of Cylindrical Geometry. *J. Chromatogr. A* **2017**, *1496*, 92–104. DOI: 10.1016/j.chroma.2017.03.048.

[40] Guiochon, G.; Marchetti, N.; Mriziq, K.; Shalliker, R. A. Implementations of Two-Dimensional Liquid Chromatography. *J. Chromatogr. A* **2008**, *1189*, 109–168. DOI: 10.1016/j.chroma.2008.01.086.

[41] Baur, J. E.; Kristensen, E. W.; Wightman, R. M. Radial Dispersion from Commercial High-Performance Liquid Chromatography Columns Investigated with Microvoltammetric Electrodes. *Anal. Chem.* **1988**, *60*, 2334–2338. DOI: 10.1021/ac00172a005.

[42] Qamar, S.; Kiran, N.; Anwar, T.; Bibi, S.; Seidel-Morgenstern, A. Theoretical Investigation of Thermal Effects in an Adiabatic Chromatographic Column Using a Lumped Kinetic Model Incorporating Heat Transfer Resistances. *Ind. Eng. Chem. Res.* **2018**, *57*, 2287–2297. DOI: 10.1021/acs.iecr.7b04555.

[43] Durbin, F. Numerical Inversion of Laplace Transforms: An Efficient Improvement to Dubner and Abate's Method. *The Comput. J* **1974**, *17*, 371–376. DOI: 10.1093/comjnl/17.4.371.

[44] Gritti, F.; Gilar, M.; Joseph, A. J. Quasi-Adiabatic Vacuum-Based Column Housing for Very High-Pressure Liquid Chromatography. *J. Chromatogr. A* **2016**, *1456*, 226–234. DOI: 10.1016/j.chroma.2016.06.029.

[45] Donald, E. P. Use of a Thermally Insulated Column for Improved Speed, Efficiency and Resolution in Packed-Column Supercritical Fluid Chromatography. *J. Chromatogr. A* **1997**, *785*, 129–134. DOI: 10.1016/S0021-9673(97)00207-0.

[46] Carslaw, H. S.; Jaeger, J. C. *Operational Methods in Applied Mathematics*; Oxford University Press: Oxford, **1953**.

[47] Chen, J.-S.; Liu, Y.-H.; Liang, C.-P.; Liu, C.-W.; Lin, C.-W. Exact Analytical Solutions for Two-Dimensional Advection-Dispersion Equation in Cylindrical Coordinates Subject to Third-Type Inlet Boundary Conditions. *Adv. Water Resour* **2011**, *34*, 365–374. DOI: 10.1016/j.advwatres.2010.12.008.

[48] Crank, J. *The Mathematics of Diffusion*, 2nd ed; Clarendon Press: Oxford, **1975**.

[49] Qamar, S.; Perveen, S.; Seidel-Morgenstern, A. Numerical Approximation of Nonlinear and Non-Equilibrium Two-Dimensional Model of Chromatography. *Comput. Chem. Eng* **2016**, *94*, 411–427. DOI: 10.1016/j.compchemeng.2016.08.008.